AIAA Guidance, Navigation, and Control Conference and Exhibit
15 - 18 August 2005, San Francisco, California

AIAA 2005-6071

Adaptive Control for a Microgravity Vibration Isolation System

Bong-Jun Yang*, Anthony J. Calise †, James I. Craig ‡

School of Aerospace Engineering, Georgia Institute of Technology

Atlanta, GA 30332

Mark S. Whorton §

Guidance, Navigation, and Mission Analysis, NASA Marshall Space Flight Center

Huntsville, AL

Abstract

Most active vibration isolation systems that try to a provide quiescent acceleration environment for space-science experiments have utilized linear design methods. In this paper, we address adaptive control augmentation of an existing classical controller that combines a high-gain acceleration inner-loop feedback together with a low-gain position outer-loop feedback to regulate the platform about its center position. The control design considers both parametric and dynamic uncertainties because the isolation system must accommodate a variety of payloads having different inertial and dynamic characteristics. An important aspect of the design is the accelerometer bias. Two neural networks are incorporated to adaptively compensate for the uncertainties within the acceleration and the position loop. A novel feature in the design is that high-band pass and low pass filters are applied to the error signal used to adapt the weights in the neural network and the adaptive signals, so that the adaptive processes operate over targeted ranges of frequency. This prevents the inner and outer loop adaptive processes from interfering with each other. Simulations show that adaptive augmentation improves the performance of the existing acceleration controller and at the same time reduces the maximal position deviation and thus also improves the position controller.

Introduction

The low-acceleration environment on the International Space Station (ISS) will enable microgravity science experiments that are practically impossible on the surface of the Earth. However, a variety of vibro-acoustic disturbances on the ISS are present and can degrade the performance of many microgravity experiments. In fact, the acceleration environment on the ISS is expected to exceed the requirements of many acceleration sensitive experiments[1] as shown in Figure 1(a). By comparing the requirement with the expected ISS acceleration in Figure 1(a), an isolation performance specification can be derived as in Figure 1(b). The isolation system must attenuate the ambient ISS acceleration by one order of magnitude at 0.1 Hz, which for a second order system implies maximum break-frequency of 0.01 Hz. That is, while the isolated system can transmit the quasi-steady accelerations of the vehicle below 0.01 Hz to the isolated assembly, it must attenuate all disturbances above 0.01 Hz. This performance specification requires the implementation of an active vibration isolation system because passive isolation systems, in general, are not able to provide sufficient attenuation of low vibration frequency disturbances.

*Postdoctoral Fellow, jun.yang@ae.gatech.edu, AIAA member
†Professor, anthony.calise@ae.gatech.edu, AIAA Fellow
‡Professor, james.craig@ae.gatech.edu, Senior AIAA member
§Branch Head, mark.whorton@nasa.gov, AIAA Associate Fellow

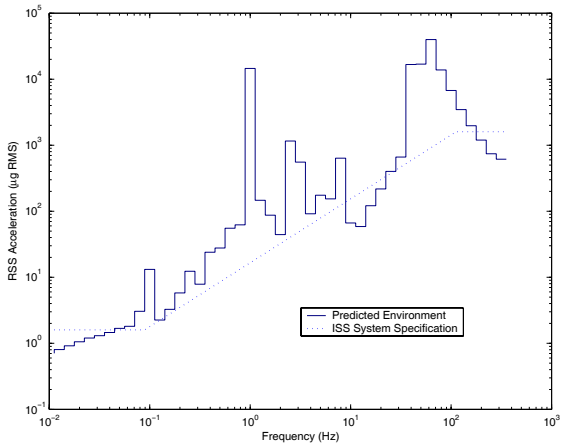

(a) Predicted RMS acceleration environment of the International Space Station

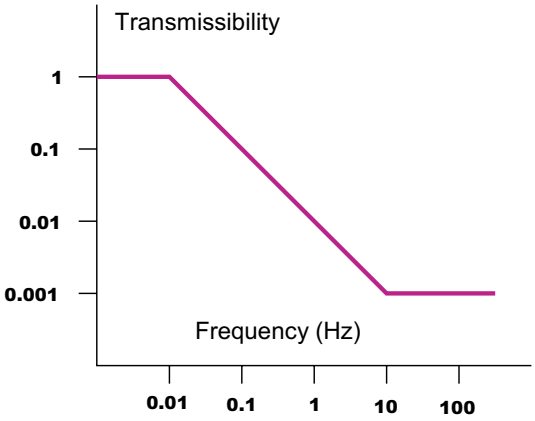

(b) Transmissibility Requirement

Figure 1. Frequency environment and requirement

An example of rack-level vibration isolation is the Active Rack Isolation System (ARIS),[2] the control architectures and flight-test results of which can be found in [3,4]. In contrast to rack-level isolation systems, g-LIMIT (gLovebox Integrated Microgravity Isolation Technology) shown in Figure 2 is a microgravity

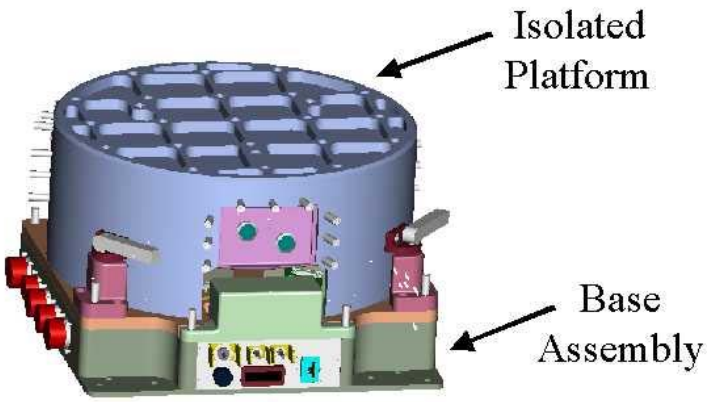

Figure 2. g-LIMIT System assembly

vibration isolation system that is designed to isolate experiments at the payload level. The g-LIMIT hardware consists of the inertially isolated assembly to which an experiment is mounted and the base assembly that is rigidly attached to the Microgravity Science Glovebox (MSG) work volume floor. In order to provide a quiescent acceleration environment for an experiment, g-LIMIT utilizes six independent control actuation channels that apply six independent magnetic forces to a platform upon which the experiment resides. g-LIMIT is designed around three integrated isolator modules (IM's), each of which is comprised of a dual-axis magnetic actuator, two axes of acceleration sensing, and two axes of sensing the relative position of the isolated platform with respect to the base assembly.[5] Integrated into the base assembly and the isolated assembly is a snubber system which provides mechanical rattle-space constraints with a maximum relative displacement of 1.0 cm between the isolated assembly and the base assembly. The only mechanical connection between the isolated platform and the base assembly is the set of umbilicals that pass resources between the MSG and the experiment.

The design of an isolation system for g-LIMIT is a challenging problem due to the stringent performance requirement and static and dynamic uncertainties that arise due both to kinematic coupling between the

platform and the mounted experiment as well as to the damping and stiffness properties of umbilicals. The mass and inertia properties of the system change considerably as various experiments utilize the isolation system during its operation. Unlike the rack-level isolation system where the rack structure is much more massive than the individual experiment, the mass and inertial variations in g-LIMIT are generally comparable to those of the isolation system and thus more problematic. The umbilicals are the primary load path for the ISS disturbances to the isolated system and the primary source of uncertainties for control system design since their stiffness and damping properties cannot be accurately measured on the ground due to gravitational deflections and coupling. Moreover, the flight-test results in [3] reveal the possibility of hysteresis in their stiffness properties. This may become a significant factor in a low-amplitude acceleration environment and may degrade the performance of the isolation system.[3]

Most vibration isolation systems have used linear control methods[6–9](an exception is found in [10]). For the design of a control system for g-LIMIT, a two-loop (inner/outer) architecture is employed. That is, a high-gain acceleration feedback is used to cancel the accelerations in the inner-loop, and a low-gain position feedback is added to the outer-loop to center the platform in the sway space and drive the platform to follow the quasi-steady motion of the vehicle. In [8], classical Proportional-Integral-Derivative (PID) controllers are designed for both the acceleration and position feedback. Fixed-order mixed H_2/μ control is considered for acceleration feedback in[9], the nominal performance and robustness of which are compared to those of a standard H_2 method.

In this paper, we consider an adaptive control approach that augments the PID control design in [8] to improve both nominal and robust performance. The adaptive elements are designed following the method described in [11, 12]. A neural network (NN) is employed to approximately cancel the uncertainty. It is well established that a NN can approximate any continuous function to any desired accuracy on a bounded set,[13] and this has been one of the main reasons given for using a NN in control approaches.[14–16] In an output feedback setting, a method that uses a memory unit of input/output delays to approximate an uncertainty has been proposed[17, 18] and shown to be effective in output feedback applications.[12, 19–21] The method in [11] is selected for the design of adaptive control for g-LIMIT because with acceleration as the regulated output, the system is nonminimum phase, and therefore inversion-based feedback approaches[22, 23] cannot be applied.

The paper is organized as follows. In Section I we present the problem of a controller design for g-LIMIT in a single-input single-output (SISO) setting. The dynamics are represented by a single mass-spring-damper system on which an experiment, modelled as two mass-spring-damper system, is mounted. In Section II, the essential features of the existing control system in [8] are presented in a SISO setting. In Section III, the details of the proposed augmenting adaptive controller design are given, with emphasis on how the approach in [11] is adapted to address the specific challenges that arise in this application. In Section IV, simulation results are described that support the validity of the overall approach. Conclusions and directions future research are given in Section V.

I. Problem Formulation

For simplicity motion along a single axis of a g-LIMIT platform on which a flexible experiment is mounted is depicted in Figure 3. The mass M_1 represents the isolated platform with a nominal experiment mass, M_2 is the uncertainty in the mass of the experiment that is mounted on the platform, and M_3 and M_4 represent flexible experiment. The term, x_o, represents the displacement of the base, x_1 is the relative displacement from the base, x_2 is the relative displacement between M_2 and M_3, and x_4 is the relative displacement between M_3 and M_4, respectively. The equation of motion for the system in Figure 3 is given by

$$\begin{aligned} &M_c(\ddot{x}_o + \ddot{x}_1) + C_1\dot{x}_1 + K_1x_1 - C_2\dot{x}_2 - K_2x_2 = u + d_1, \\ &M_3(\ddot{x}_o + \ddot{x}_1 + \ddot{x}_2) + C_2\dot{x}_2 + K_2x_2 - C_3\dot{x}_3 - K_3x_3 = d_2, \\ &M_4(\ddot{x}_o + \ddot{x}_1 + \ddot{x}_2 + \ddot{x}_3) + C_3\dot{x}_3 + K_3x_3 = d_3 \end{aligned} \tag{1}$$

where $M_c = M_1 + M_2$, and d_1, d_2, d_3 represent external disturbances applied to M_1, M_3, M_4, respectively. Two measured outputs are the *absolute* acceleration of M_1 and the *relative* displacement x_1

$$y_1 = \ddot{x}_o + \ddot{x}_1, \; y_2 = x_1. \tag{2}$$

The parameters are: $M_1 = 17.8488$, $C_1 = 0.5242$, $K_1 = 6.1574$, $M_2 = 5$, $M_3 = 5$, $M_4 = 5$, $C_2 = 1 \times 10^{-17}$, $C_3 = 1 \times 10^{-17}$, $K_2 = 15$, and $K_3 = 25$. Defining $\boldsymbol{x} = [x_1 \; \dot{x}_1, \; x_2, \; \dot{x}_2, x_3, \dot{x}_3]^T$, we can write the dynamics

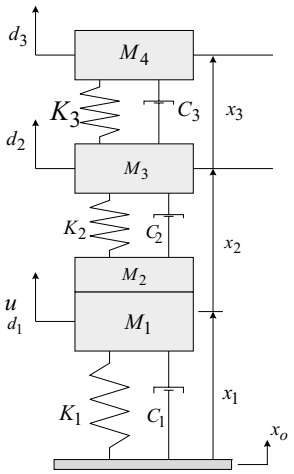

Figure 3. Mass spring damper with unmodeled dynamics

in a state space form:

$$\begin{aligned} \dot{\boldsymbol{x}} &= A\boldsymbol{x} + \boldsymbol{b}u + \boldsymbol{b}_f\ddot{x}_o + B_d\boldsymbol{d}, \quad \boldsymbol{x} \in \mathbb{R}^{6\times 1} \\ y_1 &= \boldsymbol{c}_1^T\boldsymbol{x} + Du, \\ y_2 &= \boldsymbol{c}_2^T\boldsymbol{x}, \end{aligned} \tag{3}$$

where $\boldsymbol{d} = [d_1,\ d_2,\ d_3]^T$. The plant model, which is used in the design of the feedback control system, consists of a single mass-spring-damper

$$\hat{M}(\ddot{x}_o + \ddot{x}) + \hat{C}\dot{x} + \hat{K}x = u, \tag{4}$$

where $\hat{M} = 17.8488$, $\hat{C} = 0.5242$, and $\hat{K} = 6.1574$. With the outputs corresponding to those in (2) and by letting $\boldsymbol{x}_m = [x,\ \dot{x}]^T$, the plant model can also be expressed in a state-space form:

$$\begin{aligned} \dot{\boldsymbol{x}}_m &= A_m\boldsymbol{x}_m + \boldsymbol{b}_m(u + d_1) + \boldsymbol{b}_{m_f}\ddot{x}_o, \quad \boldsymbol{x}_m \in \mathbb{R}^{2\times 1} \\ y_{m_1} &= \boldsymbol{c}_{m_1}^T\boldsymbol{x}_m + D_m u, \\ y_{m_2} &= \boldsymbol{c}_{m_2}^T\boldsymbol{x}_m. \end{aligned} \tag{5}$$

Figure 4 compares the frequency response of the plant model with that of the system in (3). The disturbance attenuation requirement in Figure 1(b) is associated with the *transmissibility*, $\frac{\ddot{x}}{\ddot{x}_o} = G_{b2a}(s)$, from the base to the isolated assembly (M_1) and shown in Figure 4(c). The control system design generally involves $G_{u2a} = \frac{y_1(s)}{u(s)}$ and $G_{u2x} = \frac{y_2(s)}{u(s)}$ which are shown in Figures 4(a) and 4(b). Note that the transfer functions from the input, u, to the acceleration and the position are the same as those from the disturbance, d_1, to the acceleration and the position since u and d_1 represent forces that are applied as the same location.

The objective of the vibration isolation system is to design a control law for u using the plant model in (5) so as to cancel the acceleration, y_1, of M_1 by an acceleration feedback while centering M_1 (*i.e.*, regulating y_2) using position feedback. The position must be restricted within a physical limit of 1.0 m. The performance of the isolation system will be measured with the control law applied to the system in (3). For the existing controller, a high-gain, high-bandwidth acceleration feedback inner-loop controller was designed to satisfy the vibration suppression requirement, and a low-gain, low-bandwidth position feedback outer-loop controller was designed to regulate position about the center in the sway space. That is, a single control is used both to suppress the acceleration and to regulate the position, and, in order to reduce the spill-over effects from one controller to the other, these controllers are designed so that the bands of frequency over which they have significant loop gain are separated.

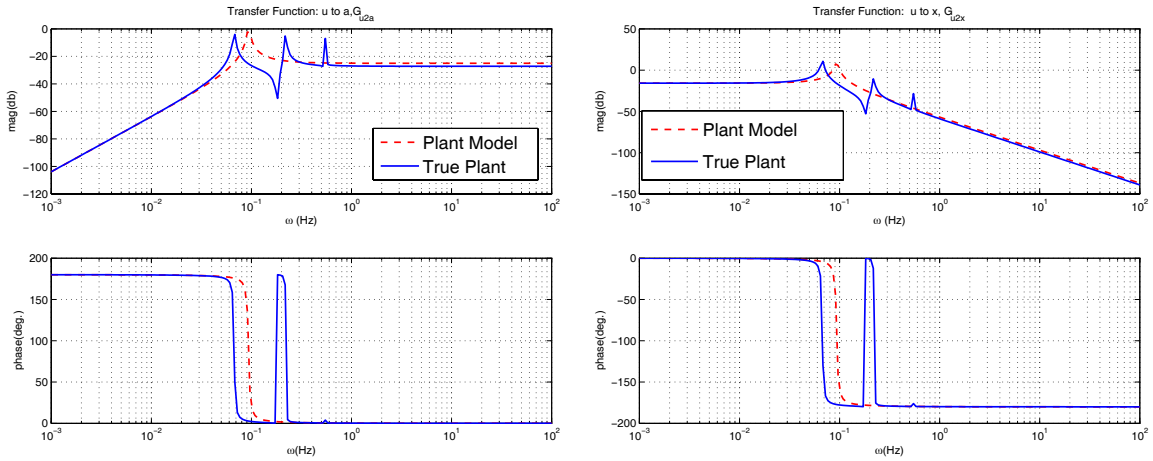

(a) Bode plot for G_{u2a} $(= \frac{y_1(s)}{u(s)})$.

(b) Bode plot for G_{u2x} $(= \frac{y_2(s)}{u(s)})$.

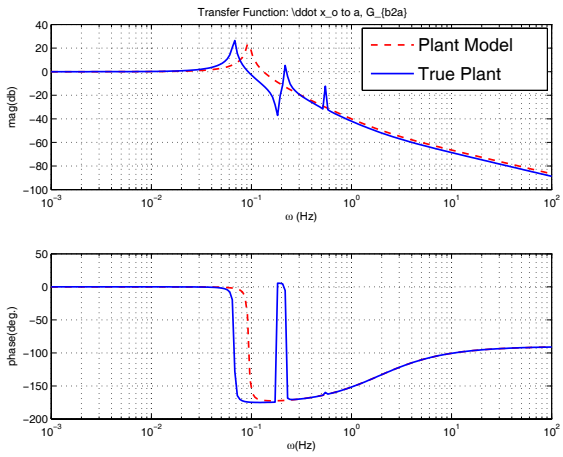

(c) Bode plot for G_{b2a} $(= \frac{y_1(s)}{\ddot{x}_o(s)})$.

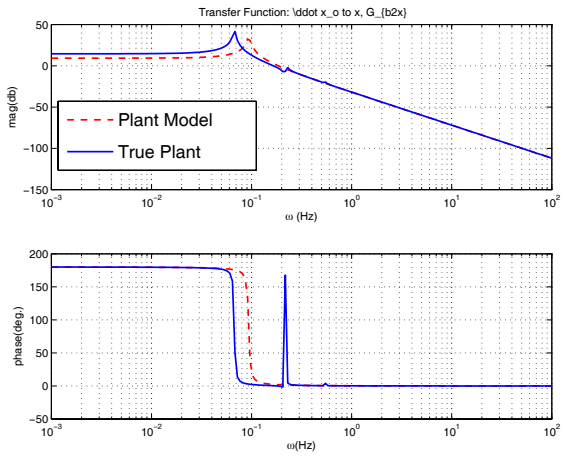

(d) Bode plot for G_{b2x} $(= \frac{y_2(s)}{\ddot{x}_o(s)})$.

Figure 4. Frequency response of various transfer functions

II. Existing Control System

A. Existing Control System

The existing control system described in [8] is shown in Figure 5. The commanded relative position (generally zero) is x_c, and n represents the accelerometer error (due to sensor bias). A PI controller is designed for the

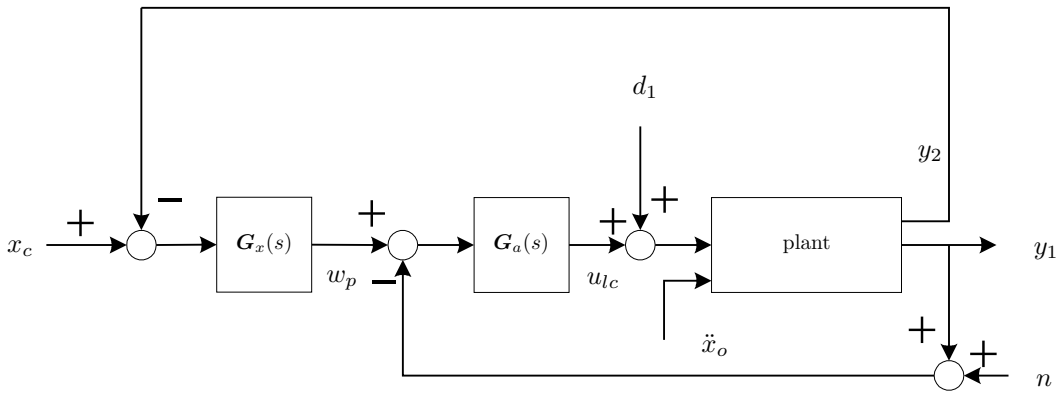

Figure 5. Existing control system architecture

inner loop

$$u_{lc} = G_a(s)\big[w_p - (y_1 + n)\big] = \frac{K_{I_i} + K_{I_p}s}{s}[w_p - (y_1 + n)], \tag{6}$$

where $K_{I_i} = 250$, and $K_{I_p} = 0.4175$. In a state space form, it is given by

$$\begin{aligned} \dot{\eta}_i &= w_p - (y_1 + n), \\ u_{lc} &= K_{I_i}\eta_i + K_{I_p}(w_p - (y_1 + n)). \end{aligned} \tag{7}$$

Applying the controller in (6) to both the plant model in (5) and the true plant in (3) leads to the frequency responses shown in Figure 6. The overall system frequency response reveals that the mounted experiment does not have much influence on the isolation system. Figure 6(c) shows that the acceleration controller is properly designed to meet the specified transmissibility. The frequency response from the sensor error to the relative position as shown in Figure 6(f) reveals an undesirable effect due to accelerometer, which suggests that without compensation the accelerometer bias can cause a large position deviation from the center of the sway space.

The outer-loop controller, $G_x(s)$ in Figure 5, is designed as a PID controller in which integral action is required to remove the effect of the accelerometer bias. Since direct implementation of derivative control amplifies the sensor noise and causes numerical problems, the PID controller is realized as

$$w_p(s) = [K_p + K_d\frac{s}{\frac{1}{50}s + 1} + \frac{K_i}{s}](x_c - y_2), \tag{8}$$

where $K_i = 3 \times 10^{-6}$, $K_d = 0.02063$, and $K_p = 0.00054$. In a state space form, it is given by

$$\begin{aligned} \dot{\boldsymbol{\eta}}_o &= A_c\boldsymbol{\eta}_o + \boldsymbol{b}_c(x_c - y_2) \\ w_p &= \boldsymbol{c}_c^T\boldsymbol{\eta}_o + D_c(x_c - y_2). \end{aligned} \tag{9}$$

Figure 7 shows the frequency response of the overall closed-loop system. On the whole, the effect of unmodelled dynamics is negligible, implying that the existing design is robust for the present case of a SISO mass-spring-damper system. Figure 7(a) indicates that the existing control system meets the performance requirement for vibration isolation. That is, if the base excitations are the only source of external disturbances, the performance of the isolation system is acceptable. Figure 7(f) indicates that the outer-loop position controller removes the effect of accelerometer bias in steady state.

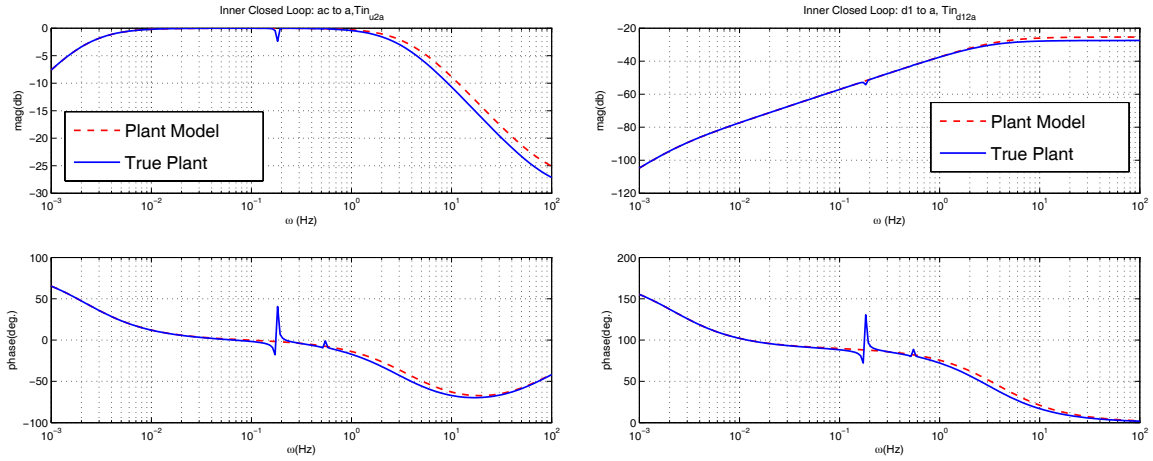

(a) Bode plot for $\frac{y_1}{w_p}$.

(b) Bode plot for $\frac{y_1}{d_1}$.

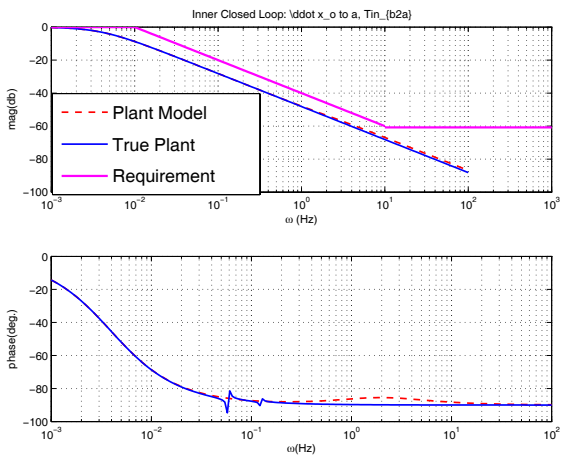

(c) Bode plot for $\frac{y_1}{\ddot{x}_o}$.

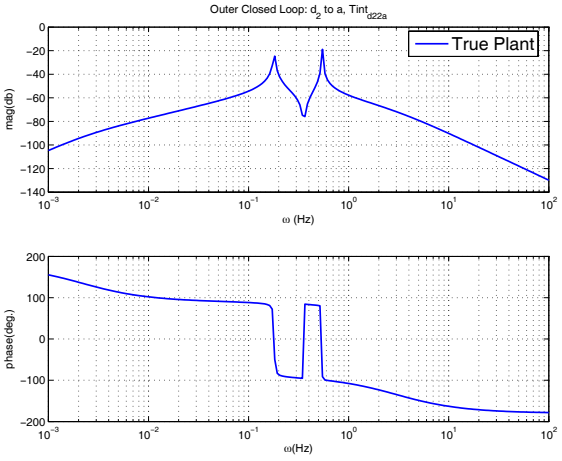

(d) Bode plot for $\frac{y_1}{d_2}$.

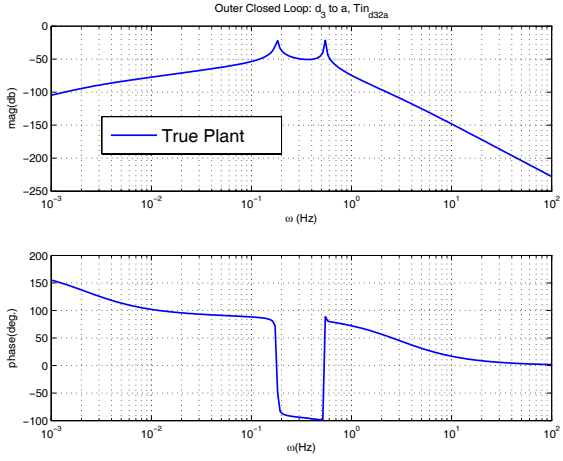

(e) Bode Plot for $\frac{y_1}{d_3}$.

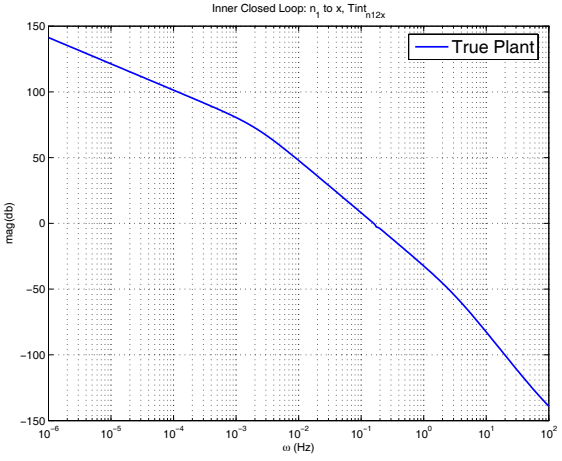

(f) Bode plot for $\frac{y_2}{n}$.

Figure 6. Frequency responses for inner-loop transfer functions

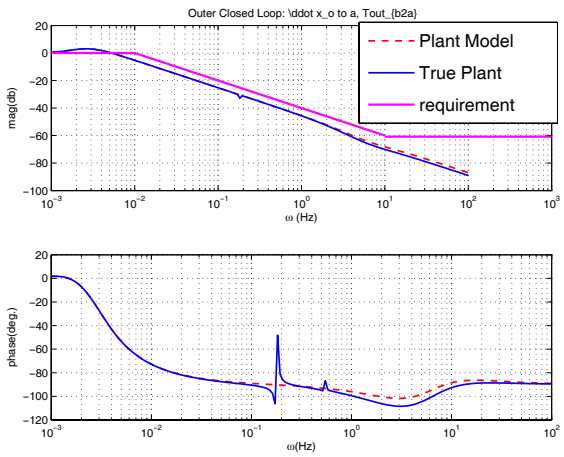

(a) Bode plot for $\frac{y_1}{\ddot{x}_o}$.

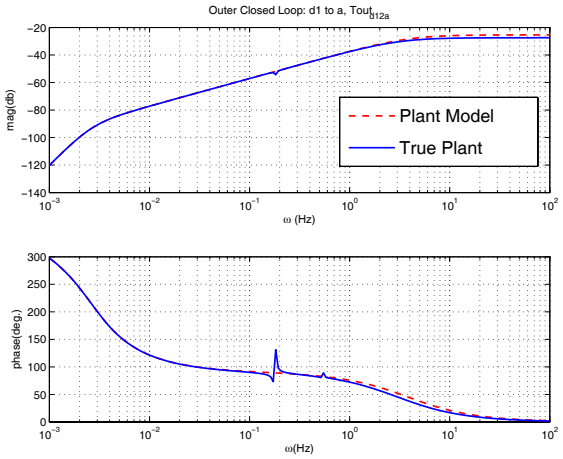

(b) Bode plot for $\frac{y_1}{d_1}$.

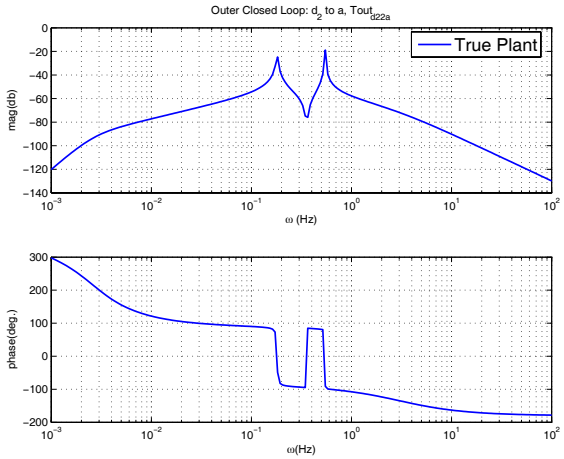

(c) Bode plot for $\frac{y_1}{d_2}$.

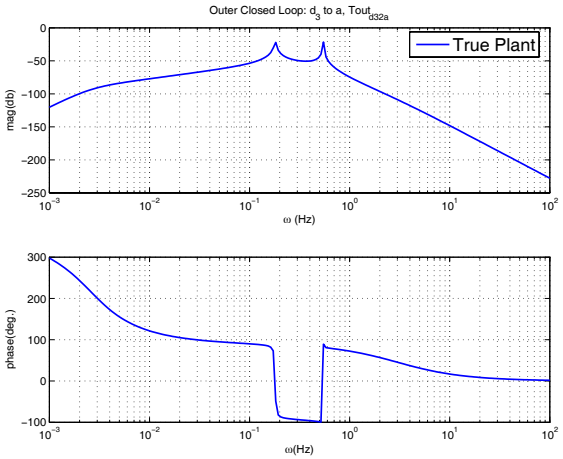

(d) Bode plot for $\frac{y_1}{d_3}$.

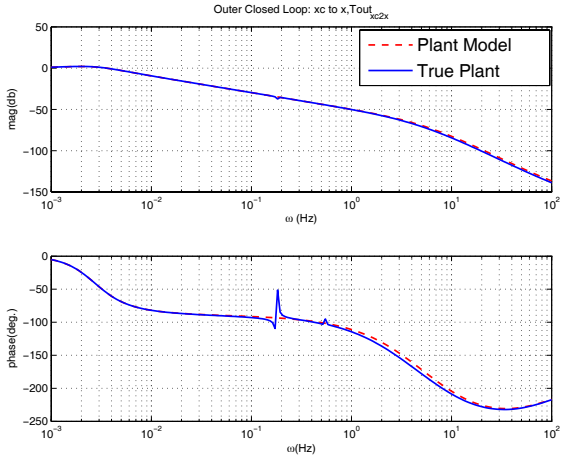

(e) Bode plot for $\frac{y_2}{x_c}$.

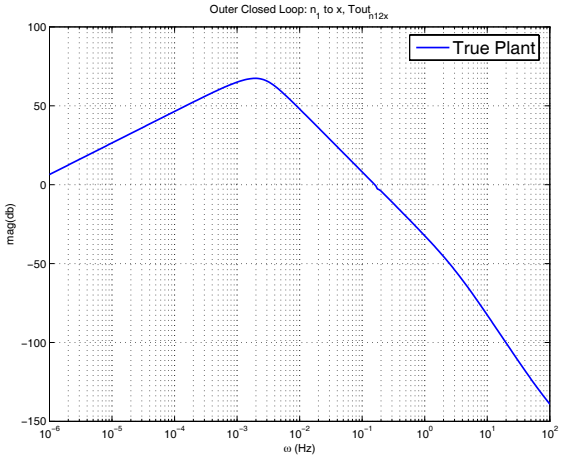

(f) Bode plot for $\frac{y_2}{n}$.

Figure 7. Frequency responses for overall (inner-loop+outer-loop) transfer functions

B. Analysis of Existing Control System

An essential feature of the existing control system in g-LIMIT is the accelerometer bias n which is is at the mili-g level, while the true acceleration is at the micro-g level. This bias is integrated by the integral action in the inner-loop and if not compensated will result in a large deviation of the isolation system in the position. This deviation is removed by the outer-loop integral action in steady space. However, transients can result in a violation of the maximal travel distance of 1.0 m. This can be avoided by increasing the gain for the outer-loop position controller, but at the expense of degrading vibration isolation performance. Therefore the objective in adding adaptation is to improve vibration isolation and position regulation. An immediate obstacle is that the acceleration output has a relative degree 0 while adaptive control methods normally require that the output has a relative degree greater than zero. Another obstacle is that only a single control is available whereas when two outputs are to be regulated. We avoid the relative degree 0 problem by a method similar to that of " dynamic extension" in [24] by designing an adaptive controller at the level of $v = \dot{u}$ for the inner-loop. To adaptively regulate two outputs, the adaptive signals for acceleration and position are separated in frequency.

With the goal of adaptive control augmentation in mind, we first provide the analysis of the closed-loop system when there exist neither modelling uncertainty nor external disturbances, i.e., $\ddot{x}_o = d_1 = 0$ in (5). This closed-loop system will ultimately be used as a reference model when introducing the adaptive controller. With dynamic extension, $\dot{\eta} = v, \eta = u$, the system in (5) is rewritten as

$$\begin{aligned} \dot{\boldsymbol{x}}_{a_m} =& A_{a_m}\boldsymbol{x}_{a_m} + \boldsymbol{b}_{a_m} v (= \dot{u}), \\ y_{m_1} =& \boldsymbol{c}_{a_{m_1}}^T \boldsymbol{x}_{a_m}, \\ y_{m_2} =& \boldsymbol{c}_{a_{m_2}}^T \boldsymbol{x}_{a_m}, \end{aligned} \tag{10}$$

where

$$\begin{aligned} & x_{a_m} = \begin{bmatrix} \eta \\ x_m \end{bmatrix},\ A_{a_m} = \begin{bmatrix} 0 & 0 \\ \boldsymbol{b}_m & A_m \end{bmatrix},\ \boldsymbol{b}_{a_m} = \begin{bmatrix} 1 \\ 0 \end{bmatrix}, \\ & \boldsymbol{c}_{a_{m_1}}^T = \begin{bmatrix} D_m & \boldsymbol{c}_{m_1}^T \end{bmatrix},\ \boldsymbol{c}_{a_{m_2}}^T = \begin{bmatrix} 0 & \boldsymbol{c}_{m_2}^T \end{bmatrix}. \end{aligned} \tag{11}$$

By defining $\boldsymbol{\xi}_m = [\xi_{m_1}\ \xi_{m_2}^1 \xi_{m_2}^2]^T = [y_{m_1},\ y_{m_2}, \dot{y}_{m_2}]^T$, the extended system in (10) can be transformed into the following normal form:[24]

$$\begin{aligned} \dot{\xi}_{m_1} &= a_{11}\xi_{m_1} + \boldsymbol{a}_{12}^T \boldsymbol{\xi}_{m_2} + D_m v, \\ \dot{\boldsymbol{\xi}}_{m_2} &= A_{22}\boldsymbol{\xi}_{m_2} + \boldsymbol{b}_{22} u, \end{aligned} \tag{12}$$

where v and u are written as if they were independent control signals, a_{11} and $\boldsymbol{a}_{12}$ are a constant scalar and a column vector, and

$$\boldsymbol{\xi}_{m_2} = \begin{bmatrix} \xi_{m_2}^1 \\ \xi_{m_2}^2 \end{bmatrix},\ A_{22} = \begin{bmatrix} 0 & 1 \\ \boldsymbol{c}_{m_1}^T \end{bmatrix},\ \boldsymbol{b}_{22} = \begin{bmatrix} 0 \\ D_m \end{bmatrix}. \tag{13}$$

When the dynamically extended system in (12) is regulated by the acceleration PI controller in (6) with $n = 0$, the inner-loop PI controller can be viewed as a PD controller as shown in Figure 8. That is, v_{lc} $(= \dot{u}_{lc})$ can be written as

$$v_{lc} = K_{I_i}\dot{\eta}_i + K_{I_p}(\dot{w}_p - \dot{y}_{m_1}) = K_{I_i}(w_p - \xi_{m_1}) + K_{I_p}(\dot{w}_p - (a_{11}\xi_{m_1} + \boldsymbol{a}_{12}^T\xi_{m_2} + D_m v_{lc})). \tag{14}$$

This leads to

$$v_{lc} = -d_{\xi_1}\xi_{m_1} - \boldsymbol{d}_{\xi_2}^T \boldsymbol{\xi}_{m_2} + d_w w_p + d_{\dot{w}}\dot{w}_p, \tag{15}$$

where

$$d_{\xi_1} = \frac{K_{I_i} + K_{I_p}a_{11}}{1 + K_{I_p}D_m},\ \boldsymbol{d}_{\xi_2}^T = \frac{K_{I_p}\boldsymbol{a}_{12}^T}{1 + K_{I_p}D_m},\ d_w = \frac{K_{I_i}}{1 + K_{I_p}D_m},\ d_{\dot{w}} = \frac{K_{I_p}}{1 + K_{I_p}D_m}. \tag{16}$$

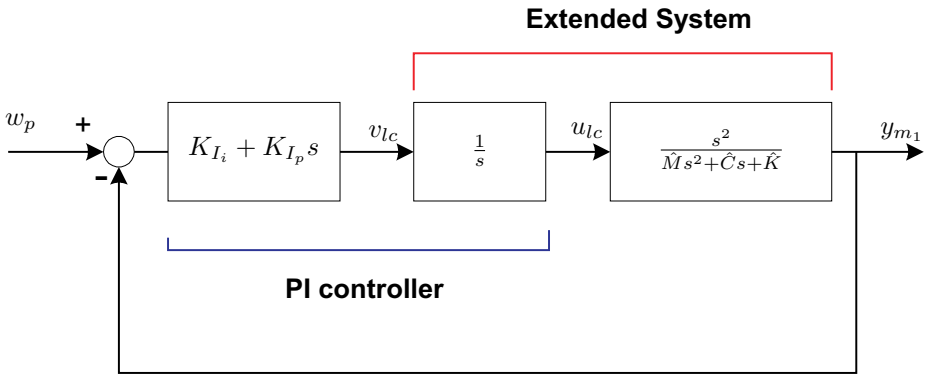

Figure 8. Inner closed-loop system

Substituting the acceleration control signal in (15) to (12) leads to

$$\begin{aligned} \dot{\xi}_{m_1} &= [a_{11} - D_m d_{\xi_1}]\xi_{m_1} + [a_{12}^T - D_m \boldsymbol{d}_{\xi_2}^T]\boldsymbol{\xi}_{m_2} + D_m[d_w w_p + d_{\dot{w}}\dot{w}_p], \quad (17) \\ \dot{\boldsymbol{\xi}}_{m_2} &= A_{22}\boldsymbol{\xi}_{m_2} + \boldsymbol{b}_{22}\left[K_{I_i}\eta_i + K_{I_p}(w_p - \xi_{m_1})\right] \quad (18) \\ \dot{\eta}_i &= w_p - \xi_{m_1}. \end{aligned}$$

Remark 1. Equations (17) and (18) reveal how the signals u_{lc} and w_p affect the acceleration and position dynamics. With $w_p = 0$, (17) shows that by selecting a high-gain K_{I_i}, the effect of $\boldsymbol{\xi}_{m_2}$ on the ξ_{m_1} dynamics can be reduced while the high-frequency ξ_{m_1} has little effect on the slow dynamics since the slow dynamics behave as a low pass filter. That is, in this case, the high-gain acceleration controller might be enough for suppressing vibration and centering the isolation system. However, when the accelerometer has a bias n, i.e., the term ξ_{m_1} in (18) is replaced by $\xi_{m_1} + n$, the bias is integrated and has a detrimental effect on the position dynamics in (18). This necessitates the design of w_p, the outer-loop controller, so as to reduce the effect of the accelerometer bias. However, the addition of w_p has also extraneous effects on the acceleration dynamics as shown in (17) and tends to degrade the performance of the acceleration controller. To minimize the effect of w_p on the acceleration dynamics, the outer-loop controller w_p is designed as a low-gain, low-bandwidth controller so that w_p and u_{lc} may be separated in bandwidths, leading to two-time scale designs for u_{lc} and w_p.

To apply w_p in (9) to (17) and (18), we require the following relation

$$\dot{w}_p = \boldsymbol{c}_c^T A_c \boldsymbol{\eta}_o + \boldsymbol{c}_c^T \boldsymbol{b}_c (x_c - \xi_{m_2}^1) + D_c(\dot{x}_c - \xi_{m_2}^2), \quad (19)$$

which leads to

$$d_w w_p + d_{\dot{w}}\dot{w}_p = \boldsymbol{g}_{\eta_o}^T \boldsymbol{\eta}_o - \boldsymbol{g}_{\xi_2}^T \boldsymbol{\xi}_{m_2} + \boldsymbol{g}_{\xi_2}^T \begin{bmatrix} x_c \\ \dot{x}_c \end{bmatrix}, \quad (20)$$

where $\boldsymbol{g}_{\eta_o}^T = d_w \boldsymbol{c}_c^T + d_{\dot{w}} \boldsymbol{c}_c^T A_c$, $\boldsymbol{g}_{\xi_2}^T = \begin{bmatrix} d_w D_c + d_{\dot{w}} \boldsymbol{c}_c^T & d_{\dot{w}} D_c \end{bmatrix}$. Combining (20) with (17) and (18) leads to the following overall closed-loop system

$$\dot{\boldsymbol{\zeta}}_m = \bar{A}\boldsymbol{\zeta}_m + B_{x_c} \begin{bmatrix} x_c \\ \dot{x}_c \end{bmatrix}, \quad (21)$$

where

$$\boldsymbol{\zeta}_m = \begin{bmatrix} \xi_{m_1} \\ \boldsymbol{\xi}_{m_2} \\ \eta_i \\ \boldsymbol{\eta}_o \end{bmatrix}, \ \bar{A} = \begin{bmatrix} a_{11} - D_m d_{\xi_1} & \boldsymbol{a}_{12}^T - D_m(\boldsymbol{d}_{\xi_2} + \boldsymbol{g}_{\xi_2})^T & 0 & D_m \boldsymbol{g}_{\eta_o}^T \\ -\boldsymbol{b}_{22} K_{I_p} & A_{22} - \boldsymbol{b}_{22} K_{I_p} D_c \boldsymbol{c}_{m_2}^T & \boldsymbol{b}_{22} K_{I_i} & \boldsymbol{b}_{22} K_{I_p} \boldsymbol{c}_c^T \\ -1 & -D_c \boldsymbol{c}_{m_2}^T & 0 & \boldsymbol{c}_c^T \\ 0 & -\boldsymbol{b}_c \boldsymbol{c}_{m_2}^T & 0 & A_c \end{bmatrix}, \ B_{x_c} = \begin{bmatrix} D_m \boldsymbol{g}_{\xi_2}^T & \\ \boldsymbol{b}_{22} K_{I_p} D_c & 0 \\ D_c & 0 \\ \boldsymbol{b}_c & 0 \end{bmatrix}. \quad (22)$$

III. Adaptive Control Augmentation

In this section we augment the inner-loop acceleration controller and the outer-loop position controller using the method in [11]. The goal is to improve the level of vibration suppression that cannot otherwise be achieved through linear control design, while satisfying the specification on the maximal travel distance for the position deviation.

A. Error Dynamics

As in the case for the plant model in (10), we extend the dynamics in (3) by defining $\dot{\eta} = v, u = \eta$. This leads to the following extended dynamics

$$\begin{aligned} \dot{\boldsymbol{x}}_a =& A_a \boldsymbol{x}_a + \boldsymbol{b}_a v + \boldsymbol{b}_{a_f} \ddot{x}_o + B_{a_d} \boldsymbol{d} \\ y_1 =& \boldsymbol{c}_{a_1}^T \boldsymbol{x}_a + D d_1 \\ y_2 =& \boldsymbol{c}_{a_2}^T \boldsymbol{x}_a \end{aligned} \tag{23}$$

where

$$\begin{aligned} &\boldsymbol{x}_a = \begin{bmatrix} \eta \\ \boldsymbol{x} \end{bmatrix},\ A_a = \begin{bmatrix} 0 & 0 \\ \boldsymbol{b} & A \end{bmatrix},\ \boldsymbol{b}_a = \begin{bmatrix} 1 \\ 0 \end{bmatrix},\ \boldsymbol{b}_{a_f} = \begin{bmatrix} 0 \\ \boldsymbol{b}_f \end{bmatrix},\ B_{a_d} = \begin{bmatrix} 0 \\ B_d \end{bmatrix} \\ &\boldsymbol{c}_{a_1}^T = \begin{bmatrix} D & \boldsymbol{c}_1^T \end{bmatrix},\ \boldsymbol{c}_{a_2}^T = \begin{bmatrix} 0 & \boldsymbol{c}_2^T \end{bmatrix}. \end{aligned} \tag{24}$$

Letting $\boldsymbol{\xi} = [\xi_1\ \xi_2^1\ \xi_2^2]^T = [y_1,\ y_2,\ \dot{y}_2]^T,\ \boldsymbol{z} = [x_3, x_2 + x_4, x_5, x_6]^T$, leads to the transformation $\begin{bmatrix} \boldsymbol{\xi} \\ \boldsymbol{z} \end{bmatrix} = T_a x_a$. With this transformation, compared to (12), the extended system in (23) can be transformed into the following normal form:

$$\begin{aligned} \dot{\xi}_1 &= a_{11}\xi_1 + \boldsymbol{a}_{12}^T \boldsymbol{\xi}_2 + D_m(v + \Delta_1), \\ \dot{\boldsymbol{\xi}}_2 &= A_{22}\boldsymbol{\xi}_2 + \boldsymbol{b}_{22}(u + \Delta_2) \\ \dot{\boldsymbol{z}} &= F_z \boldsymbol{z} + G_\xi \boldsymbol{\xi} + \boldsymbol{g}_{\ddot{x}_o} \ddot{x}_o + G_d \boldsymbol{d}, \end{aligned} \tag{25}$$

where $\boldsymbol{\xi}_2 = [\xi_2^1\ \xi_2^2]^T$, $\boldsymbol{z}$ represent the state of the stable unmodelled dynamics, and the uncertainties Δ_1 and Δ_2 are defined by

$$\begin{aligned} \Delta_1(\boldsymbol{\xi}, \boldsymbol{z}, v, \dot{d}_1, \boldsymbol{d}, \ddot{x}_o) =& \frac{1}{D_m}[\boldsymbol{c}_{a_1}^T A_a T_a^{-1} \begin{bmatrix} \boldsymbol{\xi} \\ \boldsymbol{z} \end{bmatrix} + \boldsymbol{c}_{a_1}^T \boldsymbol{b}_a v + \boldsymbol{c}_{a_1}^T \boldsymbol{b}_{a_f} \ddot{x}_o + \boldsymbol{c}_{a_1}^T B_{a_d} \boldsymbol{d} + D\dot{d}_1 - a_{11}\xi_1 - \boldsymbol{a}_{12}^T \boldsymbol{\xi}_2 - D_m v], \\ \Delta_2(\boldsymbol{\xi}, \boldsymbol{z}, \ddot{x}_o, d_1, u) =& \frac{1}{D_m}[C_{a_1} T_a^{-1} \begin{bmatrix} \boldsymbol{\xi} \\ \boldsymbol{z} \end{bmatrix} - \ddot{x}_o + D d_1 - \boldsymbol{c}_{m_2}^T \boldsymbol{\xi}_2 - D_m u]. \end{aligned} \tag{26}$$

Let

$$u = u_{lc} - u_{ad_a} - u_{ad_p}, \tag{27}$$

where u_{lc} is given by (6), u_{ad_a} is an adaptive signal to compensate for Δ_1, and u_{ad_p} is an adaptive signal to compensate for Δ_2. Similarly as in (14) and (15), applying u_{lc} in (6) leads to

$$v_{lc} = -d_{\xi_1}\xi_1 - \boldsymbol{d}_{\xi_2}^T \boldsymbol{\xi}_2 + d_w w_p + d_{\dot{w}} \dot{w}_p + \frac{K_{I_p} D_m}{1 + K_{I_p} D_m}[v_{ad_a} - \Delta_1 + \dot{u}_{ad_p}], \tag{28}$$

where $v_{ad_a} = \dot{u}_{ad_a}$. Applying (28) to (25) leads to

$$\dot{\xi}_1 = [a_{11} - D_m d_{\xi_1}]\xi_1 + [\boldsymbol{a}_{12}^T - D_m \boldsymbol{d}_{\xi_2}^T]\xi_2 + D_m[d_w w_p + d_{\dot{w}} \dot{w}_p] + \overline{D}_m[-v_{ad_a} + \Delta_1 - \dot{u}_{ad_p}], \tag{29}$$

$$\dot{\boldsymbol{\xi}}_2 = A_{22}\boldsymbol{\xi}_2 + \boldsymbol{b}_{22}\left[K_{I_i}\eta_i + K_{I_p}(w_p - \xi_1) - u_{ad_p} + \Delta_2 - u_{ad_a}\right], \tag{30}$$

$$\dot{\eta}_i = w_p - \xi_1,$$

where $\overline{D}_m = D_m(1 - \frac{K_{I_p}}{1 + K_{I_p} D_m})$.

Remark 2. Note that v_{ad_a} and u_{ad_p} are intermingled in the acceleration dynamics and position dynamics. This in general implies that v_{ad_a} and u_{ad_p} interfere with each other. One way to overcome this problem is to follow the same rationale as in the design of the existing control signals u_{lc} and w_p. v_{ad_a} is designed so that it is responsive to high frequency acceleration error, and thus should have a small effect on the low frequency position dynamics. u_{ad_p} is designed so that it is responsive to low frequency position error.

Using relations similar to those in (19) and (20), applying the outer-loop controller in (7) to (29) and (30) leads to the following overall closed-loop dynamics

$$\begin{aligned}\dot{\boldsymbol{\zeta}} &= \bar{A}\boldsymbol{\zeta} + B_{x_c}\begin{bmatrix} x_c \\ \dot{x}_c \end{bmatrix} + \underbrace{\begin{bmatrix} \overline{D}_m \\ 0 \\ 0 \\ 0 \end{bmatrix}}_{\bar{B}_v}(-v_{ad_a} + \Delta_1 - \dot{u}_{ad_p}) + \underbrace{\begin{bmatrix} 0 \\ \boldsymbol{b}_{22} \\ 0 \\ 0 \end{bmatrix}}_{\bar{B}_u}(-u_{ad_p} + \Delta_2 - u_{ad_a}) \\ \dot{\boldsymbol{z}} &= F_z\boldsymbol{z} + G_\xi\boldsymbol{\xi} + \boldsymbol{g}_{\ddot{x}_o}\ddot{x}_o + G_d\boldsymbol{d}.\end{aligned} \tag{31}$$

By defining the error vector as

$$\boldsymbol{E} = \boldsymbol{\zeta}_m - \boldsymbol{\zeta}, \tag{32}$$

comparing (31) to (21) leads to the following error dynamics

$$\begin{aligned}\dot{\boldsymbol{E}} =& \bar{A}\boldsymbol{E} + \bar{B}_v(v_{ad} - \Delta_1 - \dot{u}_{ad_p}) + \bar{B}_u(u_{ad_p} - \Delta_2 - u_{ad_a}) \\ \dot{\boldsymbol{z}} =& F_z\boldsymbol{z} + G_\xi\boldsymbol{\xi} + G_{\ddot{x}_o}\ddot{x}_o + G_d\boldsymbol{d} \\ e_1 =& y_{m_1} - y_1 = \bar{\boldsymbol{c}}_1^T\boldsymbol{E}, \\ e_2^1 =& y_{m_2} - y_2 = \bar{\boldsymbol{c}}_2^T\boldsymbol{E},\end{aligned} \tag{33}$$

where e_1 and e_2^1 represent available measurements, and $\bar{\boldsymbol{c}}_1^T = [1\ 0\ 0]$, $\bar{\boldsymbol{c}}_2^T = [0\ 1\ 0]$. Since $\bar{A}$ is Hurwitz, for any $Q > 0$, there exists a $P > 0$ such that

$$\bar{A}P + P\bar{A} + Q = 0. \tag{34}$$

The eigenvalues of the matrix $\bar{A}$ are located at $-50.0071, -13.6627, -0.0310, -0.0072 \pm 0.0068j, -0.0294$, and Q is selected as $1.5I_{6\times 6}$.

B. Adaptive Control Design

Two single hidden-layer NNs are used to approximate Δ_1 and Δ_2 in (26) which are a function of states and control. The result in [18] establishes a universal approximation for an unknown function $\Delta(\boldsymbol{x}, u)$ of states and control in a bounded, observable process using a memory unit of sampled input/output pairs. For arbitrary $\epsilon^* > 0$, there exist bounded constant weights, $\boldsymbol{M}, N$, such that:

$$\Delta(\boldsymbol{x}, u) = \boldsymbol{M}^T\boldsymbol{\sigma}(N^T\boldsymbol{\mu}) + \varepsilon(\boldsymbol{\mu}),\ |\varepsilon(\boldsymbol{\mu})| \le \epsilon^*, \tag{35}$$

where $\varepsilon(\boldsymbol{\mu})$ is the NN reconstruction error and $\boldsymbol{\mu}$ is the network input vector

$$\begin{aligned}\boldsymbol{\mu}(t) &= [\ 1 \quad \bar{\boldsymbol{u}}_d^T(t) \quad \bar{\boldsymbol{y}}_d^T(t)\ ]^T \\ \bar{\boldsymbol{u}}_d^T(t) &= [u(t) \quad u(t-d) \quad \cdots u(t-(n_1-r-1)d)]^T \\ \bar{\boldsymbol{y}}_d^T(t) &= [y(t) \quad y(t-d)\cdots y(t-(n_1-1)d)]^T\end{aligned} \tag{36}$$

in which n_1 is the length of the window and is generally required to be greater than or equal to the system dimension, $d > 0$ is a time-delay, r is the relative degree of the output, $\boldsymbol{\sigma}$ is a vector of squashing functions, $\sigma(\cdot)$, whose i^{th} element is defined as $\left[\boldsymbol{\sigma}(N^T\boldsymbol{\mu})\right]_i = \sigma\left[(N^T\boldsymbol{\mu})_i\right]$. In simulation, 4 delayed values of y_1 in (2) and 3 delayed values of the input, u, with time delay, $d = 0.025$ sec., are combined to construct the NN input signal for Δ_1. For Δ_2, the NN input is constructed in the same manner as for Δ_2 with the only difference

that the delayed values of the output y_1 is used. The squashing functions are chosen as sigmoidal functions for both networks

$$[\boldsymbol{\sigma}(N^T\boldsymbol{\mu})]_i = \frac{1}{1+e^{-a(N^T\boldsymbol{\mu})_i}},\ i=1,\ldots,6. \tag{37}$$

where $a=1$ represents the activation potential. Since we deal with two neural networks, one for the inner-loop and the other for the outer-loop, as noted in Remark 1, adaptive signals v_{ad_a} and u_{ad_p} are separated in frequency. For this reason, the design for adaptive signals involves the use of a high-pass and low-pass filter.

a high-band/low pass filter design.

1. Inner-Loop Adaptive Controller

In case of the acceleration controller, the output y_1 has a relative degree 1 with respect to the signal v. Consider the following adaptive signal used for the single NN

$$v_{ad_a} = \hat{\boldsymbol{M}}_a^T\boldsymbol{\sigma}(\hat{N}_a^T\boldsymbol{\mu}_a), \tag{38}$$

where $\hat{\boldsymbol{M}}_a$ and $\hat{N}_a$ are estimates of $\boldsymbol{M}$ and N in (35) for the case of Δ_1, and $\boldsymbol{\mu}_a$ is the NN input obtained by delayed values for y_1 and u. For the case of a relative degree 1, the NN weights can be updated as follows[21]

$$\begin{aligned}\dot{\hat{\boldsymbol{M}}}_a &= -\Gamma_{M_a}[(\hat{\boldsymbol{\sigma}}-\hat{\sigma}'\hat{N}_a^T\boldsymbol{\mu}_a)e_1P_{11}\bar{D}_m + k_a\hat{\boldsymbol{M}}_a]\\ \dot{\hat{N}}_a &= -\Gamma_{N_a}[e_1P_{11}\bar{D}_m\boldsymbol{\mu}_a\hat{\boldsymbol{M}}_a^T\hat{\sigma}' + k_a\hat{N}_a]\,,\end{aligned} \tag{39}$$

where $\Gamma_{M_a}, \Gamma_{N_a} > 0$ are positive definite adaptation gain matrices, $k_a > 0$ is a $\sigma-$modification constant, $\hat{\boldsymbol{\sigma}} \triangleq \boldsymbol{\sigma}(\hat{N}_a\boldsymbol{\mu}_a)$, $\hat{\sigma}'$ is the Jacobian computed at the estimates, and P_{11} is obtained from the decomposition of P in (34) as follows:

$$P_a = \begin{bmatrix} P_{11} & P_{21}^T & P_{31}^T \\ P_{21} & P_{22} & P_{32}^T \\ P_{31} & P_{32} & P_{33} \end{bmatrix}, \quad P_{11}\in\mathbb{R},\ P_{22}\in\mathbb{R}^{2\times2},\ P_{33}\in\mathbb{R}^{3\times3}. \tag{40}$$

However, the adaptive law in (39) becomes problematic when y_1 has a significant bias. In this case, the adaptive controller forces the biased measurement to track the reference model output, and leads to large deviation in position. At the same time is desirable that the NN not be overly responsive to high frequency sensor noise. Therefore, we introduced the following band-pass filtering of the error signal used to train the NN weights

$$e_f = H(s)e_1 = \frac{s}{(s+\omega_h)(s/\omega_M+1)}e_1, \quad \omega_h = 0.05Hz,\ \omega_M = 20Hz. \tag{41}$$

Thus e_f is used in place of e1 in (40). The following parameters are used for the adaptive law in (39)

$$\Gamma_{M_a} = 300I,\ \Gamma_{N_a} = 300I,\ k_a = 1, \tag{42}$$

where I represents the identity matrix with a compatible dimension. In implementation, the adaptive signal is also filtered through $H(s)$. Therefore, the signal v_{ad_a} is designed as

$$v_{ad_a} = H(s)[\hat{\boldsymbol{M}}_a^T\sigma(\hat{N}_a^T\boldsymbol{\mu}_a)], \tag{43}$$

leading to the following u_{ad_a} for the inner-loop acceleration controller

$$u_{ad_a} = \frac{1}{s}v_{ad_a} = \frac{1}{(s+\omega_h)(s/\omega_M+1)}[\hat{\boldsymbol{M}}_a^T\sigma(\hat{N}_a^T\boldsymbol{\mu}_a)]. \tag{44}$$

2. Outer-Loop Adaptive Controller

In case of the position controller, the output y_2 has a relative degree 2 with respect to the control u, and the approach in [11] requires an error observer for the teaching signal. In this example, the estimate for $\dot{e}_2^1$ is obtained by

$$\hat{e}_2^2 = \frac{s}{1/50s+1}e_2^1, \tag{45}$$

which results in the NN training signal $\hat{\boldsymbol{e}}_2 = [e_2^1 \ \hat{e}_2^2]^T$. As noted in Remark 1, the adaptive signal u_{ad_p} is needed to compensate for Δ_2 in the low-frequency range. To prevent interaction with u_{ad_a}, a low-pass filter is applied to the error signal

$$\hat{\boldsymbol{e}}_l = L(s)\hat{\boldsymbol{e}}_2 = \frac{1}{s/w_l + 1}\hat{\boldsymbol{e}}_2, \ w_l = 0.001Hz \tag{46}$$

and $\hat{\boldsymbol{e}}_l$ is used in place of $\hat{\boldsymbol{e}}_2$ as the error signal in the adaptive law for the outer loop NN

$$\begin{aligned} \dot{\hat{\boldsymbol{M}}}_p &= -\Gamma_{M_p}[(\hat{\boldsymbol{\sigma}} - \hat{\sigma}'\hat{N}_p^T\boldsymbol{\mu}_p)\hat{\boldsymbol{e}}_l P_{22}\boldsymbol{b}_{22} + k_p\hat{\boldsymbol{M}}] \\ \dot{\hat{N}}_p &= -\Gamma_{N_p}[\hat{\boldsymbol{e}}_l P_{22}\boldsymbol{b}_{22}\boldsymbol{\mu}_p\hat{\boldsymbol{M}}_p^T\hat{\sigma}' + k_p\hat{N}_p] \end{aligned} \tag{47}$$

where P_{22} is obtained from (40), and $\boldsymbol{\mu}_p$ is the NN input obtained by delayed values for y_2 and u. The tuning parameters for the NN are

$$\Gamma_{M_p} = 1 \times 10^{-4}I, \ \Gamma_{N_p} = 1 \times 10^{-4}I, \ k_p = 3 \times 10^4. \tag{48}$$

The signal u_{ad_p} is also filtered through the low-pass filter in (46). The adaptive signal u_{ad_p} is given by

$$u_{ad_p} = L(s)[\hat{\boldsymbol{M}}_p^T\sigma(\hat{N}_p^T\boldsymbol{\mu}_p)]. \tag{49}$$

Figure 9 shows the frequency responses of the band-pass filter in (41) and the low-pass filter in (46). The

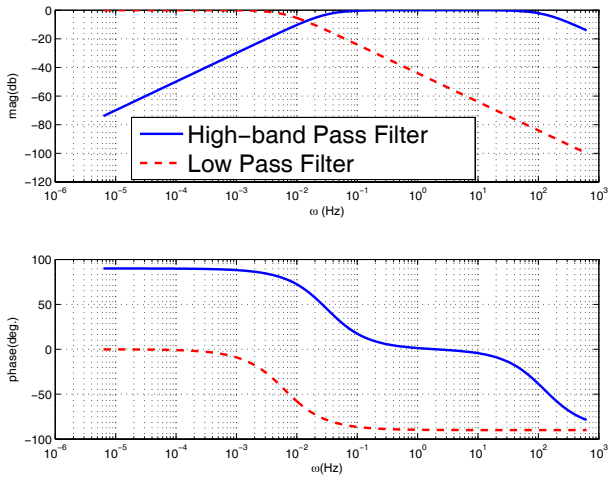

Figure 9. Frequency Responses of Filters used in Adaptive Control Design

overall architecture for the adaptive control augmentation is depicted in Figure 10, in which abbreviations are defined as follows:" TP" for the true plant in (3), "PM" for the plant model in (5) with $\ddot{x}_o = n = 0$, " BP " for the band-pass filter in (41), " LP " for the low-pass filter in (46), "NN_a " for the NN in the acceleration inner-loop, and "NN_p" for the NN in the position outer-loop.

IV. Simulation Results

When x_c is set to zero the reference model generates $y_{m_1} = y_{m_2} = 0$ and need not be implemented. The accelerometer bias for y_1 is set at 0.001 m/sec (=102 μ g). Figure 11 shows the acceleration response y_1 and the position response y_2 with the base excitation, $\ddot{x}_o = 16\mu g \sin(2\pi(0.067)t)$ in the absence of sensor bias. The base excitation frequency corresponds to the first flexible mode in the open-loop system in Figure 4(c), thus the open-loop system ("OL") exhibits greatly amplified responses ($|G_{b2a}(j\omega)|_{\omega=0.067Hz} \simeq 25dB$) to the given base excitation. With the existing control system ("EC without sensor bias"), the transmissibility is -20 dB as shown in Figure 7(a), and the acceleration is significantly attenuated. Figure 11(b) also shows that the position oscillates with a small magnitude around zero, and its magnitude is much smaller than the maximal travel distance limit 1.0 m.

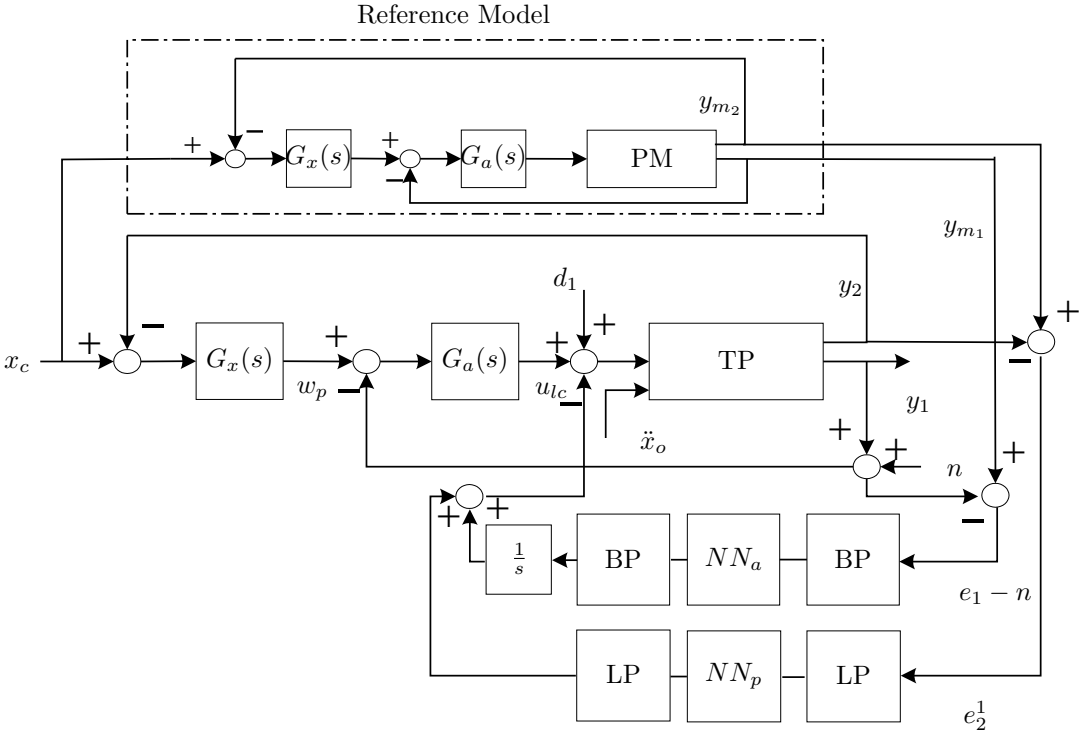

Figure 10. Adaptive Control Augmentation Architecture

The situation greatly changes when the 1.0 mili-g sensor bias is introduced. Figure 12 compares the responses of the acceleration and the position with and without the sensor bias ("EC" and " EC without sensor bias", respectively). Note that the transient position error violates the 1.0 m limit. However, notice that in steady-state, the position error converges to zero, and the same level of the acceleration is recovered as that with the existing control system without the sensor bias.

Figure 13 compares the responses of the acceleration and the position when the system in (3) is regulated by the existing control system ("EC"), the existing control system augmented by the inner-loop adaptive controller ("EC+u_{ad_a}"), and the existing control system augmented by both the inner-loop and outer-loop adaptive controllers ("EC+$u_{ad_a} + u_{ad_p}$") for 3000 seconds. The inner-loop adaptive controller enhances the isolation performance while the relative position is regulated at the same level as the existing control system. This indicates that the inner-loop adaptive controller is active only at high-frequency bands and has little effect on the position dynamics. However, it still violates the distance limit for the isolation system. Figure 13(b) shows that adding the outer-loop adaptive controller improves the response so that the limit on peak response is satisfied, with a modest increase in the peak acceleration. Figure 14(a) shows the transient response for the initial 250 seconds. In the transient responses, oscillations occur at 0.05 Hz, reflecting the effect of the band-pass filter in (41) for the adaptive signal v_{ad_a}. Figure 14(b) shows that in steady-state, as the position deviation converges to zero, the effect of u_{ad_p} diminishes, and the augmented control system retains the same performance as that of the inner-loop adaptive controller without the outer-loop adaptive controller.

Assessment of the isolation performance throughout the specified frequency range requires the development of a performance measure that quantifies how much the transmitted acceleration is attenuated in a nonlinear system. In this example, steady-state responses are recorded after the transient responses decay, and the attenuation level similar to Figure 7(a) are found by extrapolating the recorded data. The base excitation ranges from $1.6\mu g$ to $1.6 \times 10^3 \mu g$ following the predicted ISS acceleration environment in Figure 1(a). The result is plotted in Figure 15. According to the attenuation requirement in Figure 1(b), active isolation is only required in the range of 0.01 Hz-10 Hz because the base excitations below 0.01 Hz must be transmitted to the isolated platform in order for the isolated system to move with the vehicle, and the open-loop system satisfies the performance requirement above 10 Hz. Figure 15 show that the adaptive

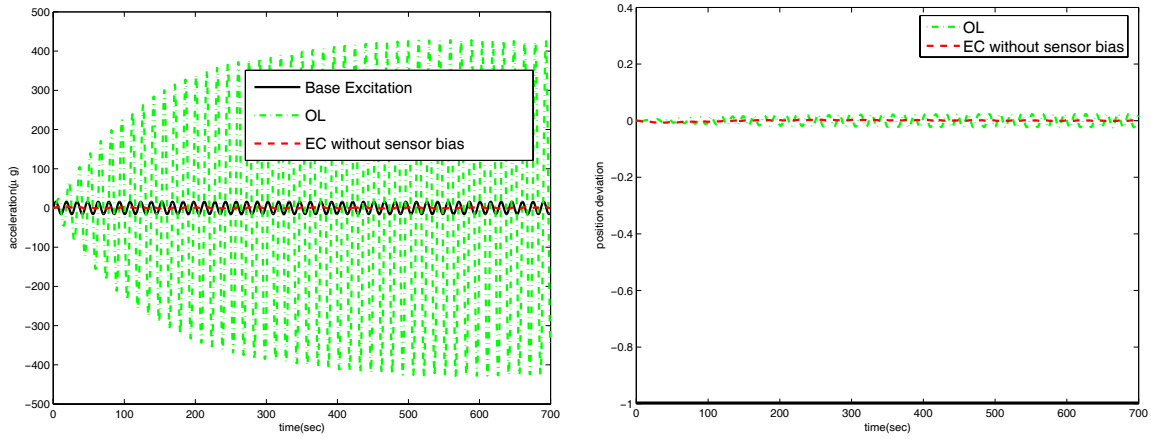

(a) Acceleration response y_1 (b) Position response y_2

Figure 11. Responses with the base excitation $\ddot{x} = \sin 2\pi(0.067)t$ WITHOUT sensor bias

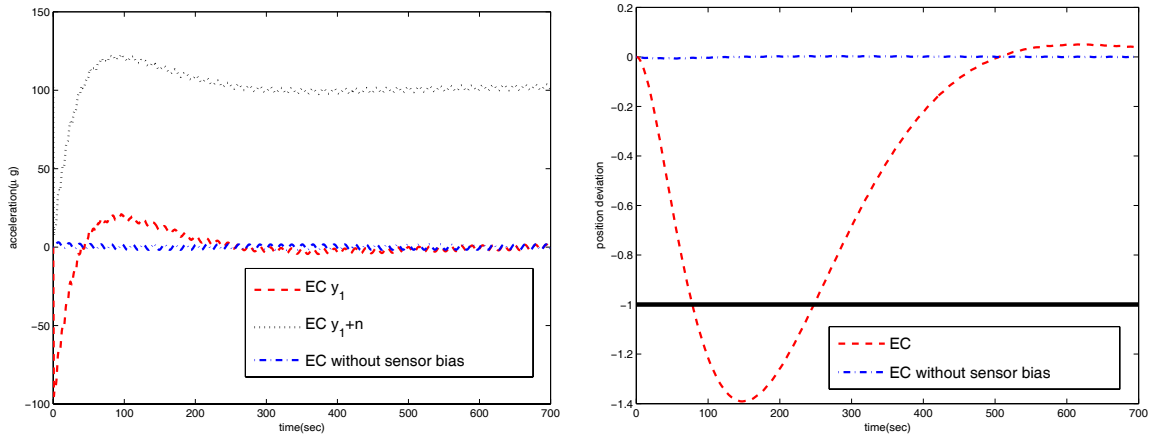

(a) Acceleration response y_1 (b) Position response y_2

Figure 12. Comparison of responses with the existing control system with and without accelerometer when $\ddot{x}_o = 16\mu g \sin(2\pi(0.067)t)$

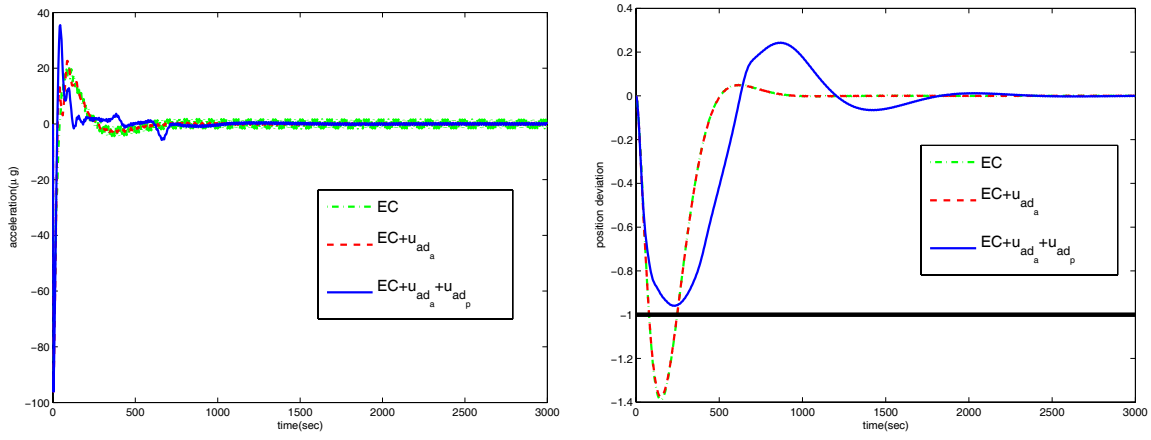

(a) Acceleration response y_1 (b) Position response y_2

Figure 13. Responses with the existing controller augmented by the adaptive controllers when $\ddot{x}_o = 16\mu g \sin(2\pi(0.067)t)$

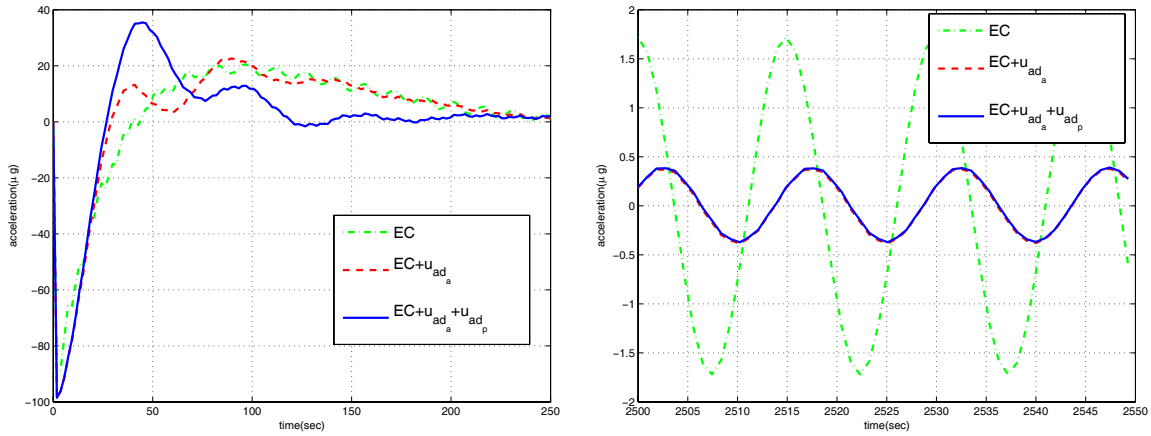

(a) Transient response y_1 (b) Steady-state response y_1

Figure 14. Transient and steady-state acceleration response when $\ddot{x}_o = 16\mu g \sin(2\pi(0.067)t)$

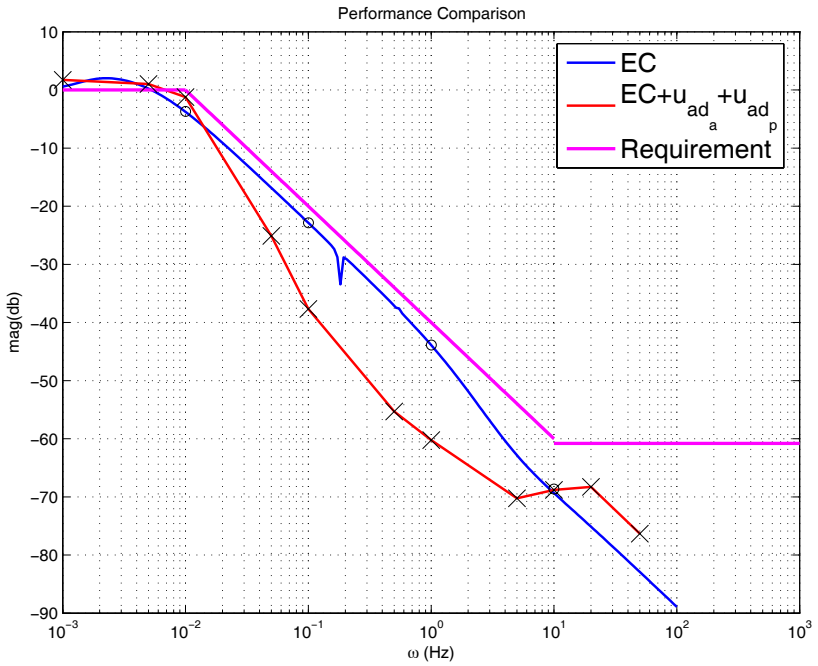

Figure 15. Comparison of performance in various frequencies

controller outperforms the existing control system throughout the frequency range of 0.01 Hz-10 Hz. That is, the adaptive control system promises its main benefits in the critical frequency range in which parametric uncertainties related to the inertia properties and the umibilical stiffness are expected to change the shape of the frequency responses shown in Figure 4. For example, the flight-test results in [3] show that the linear design fails to meet the performance requirement in the range of 0.04 Hz-0.4 Hz due to the hysteresis in the umbilical stiffness. The present results suggest that with adaptive augmentation the linear controller may be able to meet these requirements.

Investigating the frequency responses of $\frac{y_1}{d_1}$, $\frac{y_1}{d_2}$, and $\frac{y_1}{d_3}$ in Figures 7(b), 7(c), and 7(d) reveals that at high frequencies (above 1 Hz), the external disturbance d_1 is most influential (-30dB) among the external disturbances d_1, d_2, and d_3, which could arise when the experiment mounted on the isolated platform has its own source of vibration. Disturbances d_2 and d_3 lead to -40dB gain over all frequencies, and thus are negligible disturbance sources. Figure 16 shows the acceleration responses when disturbances d_1 =

$16\mu g \sin(2\pi 0.1(Hz)t)$ and $d_1 = 160\mu g \sin(2\pi 5(Hz)t)$ are applied. At 0.1 Hz, $|\frac{y_1}{d_1}(j\omega)|$ is close to $-10dB$ for

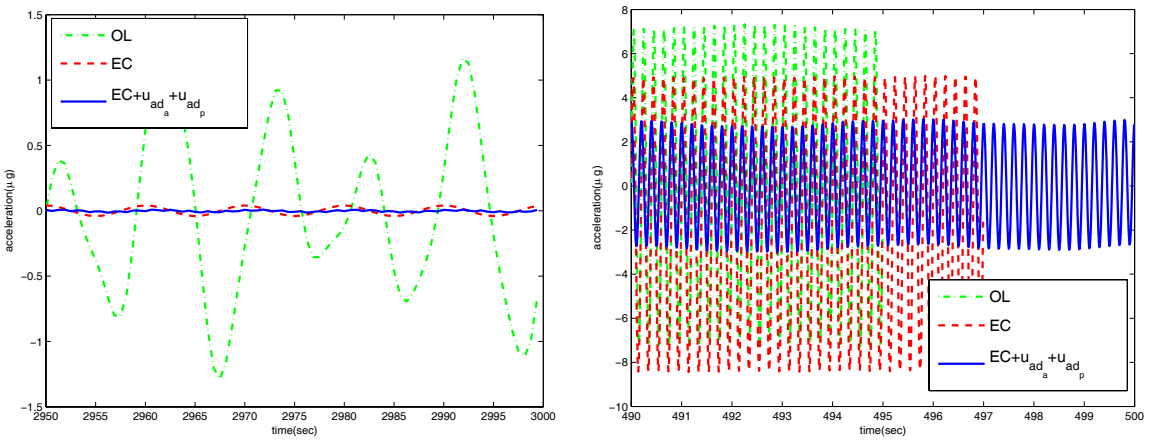

(a) Acceleration response with $d_1 = 16\mu g \sin(2\pi 0.1(Hz)t)$

(b) Acceleration responses with $d_1 = 160\mu g \sin(2\pi 5(Hz)t)$

Figure 16. Acceleration Responses with Direct Disturbance d_1

the open-loop system and $-50dB$ for the system regulated by the existing controller as shown in Figures 4(a) and 7(b). Thus, the existing control system is very effective in rejecting d_1 disturbances at this frequency. The adaptive controller achieves similar performance to that with the existing control system as shown in Figure 16(a). Figure 16(b) shows that at a frequency of 5.0 Hz, the adaptive controller improves the performance of the existing controller. Since $|\frac{y_1}{d_1}(j\omega)|_{\omega=5Hz}$ is close to $-30dB$ for both the open-loop system and the system with the existing controller, the acceleration responses exhibit the same magnitude of oscillation in steady-state response. With the adaptive control, the acceleration is greatly suppressed. Similarly as in the case of the base excitation, adaptive control generally improves performance of the existing control system between 0.1 Hz and 10 Hz in the presence of d_1 disturbances.

V. Conclusions and Future Work

We consider adaptive control augmentation of an existing linear controller for g-LIMIT. Both the acceleration control loop and the position control loop are augmented with adaptive elements that are designed based on two-time scales, similar to the approach taken in designing the existing control system. Introducing band-pass filtering of the error signals used in the adaptive laws prevents interactions between the NNs used in each loop. The adaptive control system outperforms the existing control system in the range of 0.1 Hz and 10 Hz in attenuating both the base excitation and the direct disturbance to the isolation system while meeting the specification for the position deviation, under the same conditions that cause a violation when using the existing control design.

As a next step, we plan to extend the current SISO result to a MIMO system in a more realistic simulation environment for g-LIMIT provided by NASA Marshall Space Flight Center.

Acknowledgments

This research was supported by the NASA Marshall Space Flight Center, under grant number NAG8-1912. The authors would like to thank Dr. Young Kim at MSFC and Nathan Graybeal at Georgia Tech. for their collaboration on this research.

References

[1]Del Basso, S. and Bogert, P. B., "The Space Station Freedom Microgravity Environment," AIAA-1993-0831, January 1993.

[2]Bushnell, G. S., Anderson, T. M., Becraft, M. D., and Jacot, A. D., "Microgravity Performance Flight Characterization of an International Space Station Active Rack Isolation Prototype System," *AIAA/ASME/ASCE/AHS/ASC Structures,*

Structural Dynamics, and Materials Conference and Exhibit, 38th, and AIAA/ASME/AHS Adaptive Structures Forum, AIAA 1997-1203, Kissimmee, FL, April 1997.

[3]Bushnell, G. S. and Becraft, M. D., "Microgravity Performance Flight Characterization of an International Space Station Active Rack Isolation Prototype System," *Proceedings of the 16th IEEE Instrumentation and Measurement Technology Conference*, Vol. 1, May 1999, pp. 260 – 267.

[4]Moss, L., Just, M., Grodsinsky, C., Heese, J., and Humphreys, B., "Microgravity Environment Predictions and Control for the Fluids Integrated Rack," *AIAA Aerospace Sciences Meeting*, AIAA 2004-5019, Reno, NV, January 2004.

[5]Kim, Y. and Whorton, M. S., "Equations of Motion for the g-LIMIT Microgravity Vibration Isolation System," Tech. Rep. NASA TM-1999-209009, January 1999.

[6]Grodsinsky, C. M. and Whorton, M., "A Survey of Active Vibration Isolation Systems for Microgravity Applications," *AIAA Journal of Spacecraft and Rockets*, Vol. 37, No. 8, Sep.-Oct. 2000.

[7]Calhoun, P. C. and Hampton, R. D., "Optimal Control Design using an H_2 Method for the Glovebox Integrated Microgravity Isolation Technology (g-LIMIT)," *Proceedings of AIAA guidance,navigation and control conference*, AIAA 2002-5020, Monterey, CA, August 2002.

[8]Jackson, M., Kim, Y., and Whorton, M., "Design and Analysis of the g-LIMIT Baseline Vibration Isolation Control System," *Proceedings of AIAA guidance,navigation and control conference*, AIAA 2002-5019, Denver, Co, August 2002.

[9]Whorton, M., "Robust Control for the g-LIMIT Microgravity Vibration Isolation System," *AIAA Journal of Spacecraft and Rockets*, Vol. 42, No. 1, 2005.

[10]Shkolnikov, I., Shtessel, Y., Whorton, M. S., and Jackson, M., "Microgravity Isolation Control System Design via High-Order Sliding Mode Control," *Proceedings of the American Control Conference*, Chicago, IL, June 2000, pp. 2072–2076.

[11]Hovakimyan, N., Yang, B.-J., and Calise, A., "An Adaptive Output Feedback Control Methodology for Non-Minimum Phase Systems," *Proceedings of Conference on Decision and Control*, Las Vegas, NV, 2002, pp. 949–954.

[12]Yang, B.-J., Hovakimyan, N., Calise, A., and Craig, J., "Experimental Validation of an Augmenting Approach to Adaptive Control of Uncertain Nonlinear Systems," *Proceedings of AIAA guidance,navigation and control conference*, AIAA-2003-5715, Austin, TX, 2003.

[13]Hornik, N., Stinchcombe, M., and White, H., "Multilayer feedforward networks are universal approximators," *Neural Networks*, Vol. 2, 1989, pp. 359–366.

[14]Ge, S., Lee, T., and Harris, C., *Adaptive Neural Network Control of Robotic Manipulators*, World Scientific, 1998.

[15]Lewis, F., Jagannathan, S., and Yeşildirek, A., *Neural Network Control of Robot Manipulators and Nonlinear Systems*, Taylor & Francis, 1999.

[16]Spooner, J. T., Maggiore, M., Ordóñez, R., and Passino, K. M., *Stable Adaptive Control and Estimation for Nonlinear Systems- Neural and Fuzzy Approximator Techniques*, John Wiley & Sons, New York, NY, 2002.

[17]Hovakimyan, N., Nardi, F., Calise, A., and Lee, H., "Adaptive Output Feedback Control of a Class of Nonlinear Systems Using Neural Networks," *International Journal of Control*, Vol. 74, No. 12, 2001, pp. 1161–1169.

[18]Lavretsky, E., Hovakimyan, N., and Calise, A., "Upper Bounds for Approximation of Continuous-Time Dynamics Using Delayed Outputs and Feedforward Neural Networks," *IEEE Transactions on Automatic Control*, Vol. 48, No. 9, 2003, pp. 1606–1610.

[19]Kim, N., Calise, A. J., Hovakimyan, N., Prasad, J., and Corban, J. E., "Adaptive Output Feedback for High-Bandwidth Flight Control," *AIAA Journal of Guidance, Control & Dynamics*, Vol. 25, No. 6, 2002, pp. 993–1002.

[20]Calise, A., Yang, B.-J., and Craig, J., "An Augmenting Adaptive Approach to Control of Flexible Systems," *AIAA Journal of Guidance, Control & Dynamics*, Vol. 27, No. 3, 2004, pp. 387–396.

[21]Yang, B.-J., Calise, A., and Craig, J., "Adaptive Output Feedback Control of a Flexible Base Manipulator," *Proceedings of AIAA guidance,navigation and control conference*, AIAA-2004-5322, Providence, RI, August 2004.

[22]Calise, A., Hovakimyan, N., and Idan, M., "Adaptive Output Feedback Control of Nonlinear Systems using Neural Networks," *Automatica*, Vol. 37, No. 8, 2001, pp. 1201–1211.

[23]Hovakimyan, N., Nardi, F., Kim, N., and Calise, A., "Adaptive Output Feedback Control of Uncertain Systems using Single Hidden Layer Neural Networks," *IEEE Transactions on Neural Networks*, Vol. 13, No. 6, 2002.

[24]Isidori, A., *Nonlinear Control Systems II*, Springer-Verlag, London, 1999.